Korean J. Chem. Eng., **26**(5), 1365-1372 (2009)
DOI: 10.1007/s11814-009-0211-x

Salt-induced protein separation in an aqueous electrolyte solution

Sang Ha Choi and Young Chan Bae†

Division of Chemical Engineering and Molecular Thermodynamics Laboratory,
Hanyang University, Seoul 133-791, Korea
(*Received 11 January 2009 • accepted 17 February 2009*)

Abstract−Liquid-liquid phase separations of aqueous ovalbumin and bovine serum albumin (BSA) solutions are reported experimentally for a wide range of solution conditions. The temperature-induced clouding of protein solutions, which signals the onset of liquid-liquid phase separation, provides a simple means of assessing the effect of solution conditions on the strength of protein interaction. Our results show that the effect of salts on protein interactions depends sensitively on the ionic composition of solution and the identities of both the cation and the anion of the added salts. The results are used to test and refine theoretical models for the interaction energy between macromolecules. A modified perturbed hard-sphere chain (MPHSC) model is employed to determine the interaction energy for solvation forces playing an important role in protein interactions and to predict the osmotic pressures of protein solutions.

Key words: BSA, Ovalbumin, Liquid-liquid Phase Separation, Cloud-point Temperature (CPT), MPHSC

INTRODUCTION

Molecular thermodynamics has applications in bioprocessing in a number of areas, including purification of biological molecules and drug delivery. It also serves as the basis for understanding and performing intracellular events such as signal transduction, and determining optical conditions for protein folding, for separation of protein mixtures and for crystallization through understanding protein-protein intermolecular forces. Similarly, the phase behavior of protein solution is determined by both intra- and intermolecular interactions. Information about protein phase diagrams is especially important for the design of protein purification and separation processes by precipitation, which is the first and most common step in protein isolation. The two general kinds of phase transitions of interest are crystallization and liquid-liquid phase separation; however, the latter often occurs under meta-stable conditions [1-9].

Liquid-liquid phase separation has been studied extensively in liquid mixtures, in polymer solutions, and in micellar solutions. Wolde and Frenkel [10] have reported that the free energy barrier for crystal nucleation is remarkably reduced at the critical point of liquid-liquid phase separation. In general, after liquid-liquid phase separation, crystallization occurs much more rapidly than in the initial solution. Therefore, the determination of the location of liquid-liquid phase separation curve is very effective for identifying the optimum solution conditions for growing protein crystals. We have performed a particular challenge that the phenomenon of liquid-liquid phase separation lies in quantifying and revealing the changes in the interaction energy of the biological molecules. This finding is useful for understanding how protein behaves under a variety of solution conditions.

Proteins are water soluble bio-macromolecules and have two main structural patterns: those that contain hydrophilic sites that can stabilize the aqueous solution by forming hydrogen bonds with the neighboring water molecules, and hydrophobic sites that can be destabilized aqueous solution through their aggregation and the release of the surrounding water molecules. Rupert [11] interprets the cloud-point phenomenon as the result of the balance between the hydrophobic and hydrophilic interactions of a particle with its surroundings in water/nonionic surfactant systems. The cloud-point phenomenon has been reported to a boundary that protein solution can be reversibly altered by the presence of electrolytes, which may be often in case of two phase separation, such as salt-induced precipitation [12-16]. In possibility, protein is partitioned to the protein-rich phase when the solution is heated or cooled above a certain added to enhance the partition of protein at room temperature, and the other is depleted.

In traditional colloidal characterization techniques, some aspects of the interactions in protein solutions have been studied separately by scattering methods-static light scattering (SLS) [17], dynamic light scattering (DLS) [18], x-ray scattering [19], low-angle laser-light scattering (LALLS) [20,21], and small-angle neutron scattering (SANS) [22] that have been applied to characterize the protein crystallization as well as the liquid-liquid phase separation, but these methods are time consuming and need a great amount of protein. For aqueous solutions of ovalbumin and BSA, we obtained liquid-liquid phase separation data by thermo-optical analysis (TOA) apparatus. Thermal analysis is the simplest and oldest analytical method and is powerful a tool in the hands of polymer scientists to illustrate the non-equilibrium effects which are typical of solutions.

In this work, aqueous protein solutions are partitioned into two liquid phases by the addition of relatively small amount of electrolytes. We employ low protein concentrations to distinguish aggregation, and study liquid-liquid phase separation through measuring CPT by using the salting-out method from aqueous solutions. We developed a new analytical perturbation equation of state by introducing the generalized Lennard-Jones potential (GLJ) to explain the short-range interaction between proteins. In addition, we dem-

†To whom correspondence should be addressed.
E-mail: ycbae@hanyang.ac.kr

onstrate that the new EOS is capable of predicting the osmotic pressure of the real protein solutions with agreement.

MATERIALS AND METHODS

1. Protein/Salt Solution Preparation

Ovalbumin from Grade VI, approx. 99% (agarose gel electrophoresis), lyophilized powder, bovine serum albumim (BSA) from pH 7, suitable for diluent in ELISA applications, min. 98% (electrophoresis), lyophilized powder, reagent-grade NaCl, $NaNO_3$, NH_4Cl, $MgCl_2$, Na_2SO_4, tris buffer, sodium azide were from Sigma and Aldrich. A 1 L stock solution of 20 mM tris buffer was prepared and sodium azide was then added to the protein solution at a concentration of 2 mM to prevent bacterial growth. The stock solution was preserved at 4 °C with enclosing. Protein was dissolved in a small volume of the stock solution. A salt was added with desired concentration and then stirred. The pH of the solution was checked after mixing, and adjusted with concentrated 1N-HCl or 1N-NaOH.

To conduct our experiments, we used the routine filling methods reported by Park et al. [23], and Malcolm and Rowlinson [24]. After stirring protein-salt solutions for ~2 hr, a desired sample was filled in slim pyrex capillary with 0.02-0.03 mL by plastic needle syringe. The sample tube was collapsed and sealed when one end was heated by a flame while the content of the tube was maintained at a subambient temperature by liquid nitrogen.

2. Determination of Liquid-liquid Phase Separation

An effective way to determine the strength of protein interactions is to study temperature-induced phase transitions that occur in protein solutions. Crystallization and phase transition in liquid crystalline solutions were directly determined by TOA. TOA techniques have been used to measure physical properties of a sample as a function of temperature while the sample is subjected to a controlled temperature program [25-27]. A sample is heated by a constant heat flow rate, and any phase transition is recorded as invariance in temperature, and additional information about the nature of the phase transitions is obtained. The features of this apparatus, which is used to characterize protein interactions, require only commonly available laboratory equipment and little specialized expertise. TOA also provides powerful, rapid and reliable experimental results. In this work, it was used with very small samples and a relatively small investment in running time.

TOA was performed by using a polarized light microscope equipped with a hot-stage by which the temperature of a sample could be controlled. Temperature was plotted on decreasing upwards, and time on the abscissa increases from left to right. A sample is proportionally imposed on temperature program against time, in an environment heated at a controlled rate. The temperature program was used with a METTLER FP90 central processor consisting of a starting temperature, heating and cooling rate, and an end temperature. The temperature of the system can be varied from −60 to +350 °C with scan rates as low as 0.1 °C/min for both heating and cooling. The image of the sample can be viewed directly in binoculars, and the transmitted light intensity as a function of temperature is recorded by a photodiode. Results are connected to an IBM PC for data storage, and this data is used to determine the cloud points.

The temperature at which a homogenous aqueous protein solution starts to turn cloudy by temperature program is referred to as the cloud-point temperature (CPT) which corresponds to a remarkable decrease of light intensity. At the occurrence of cloudiness, macroscopic phase separation with a dilute and concentrated protein was observed, i.e., aggregation in protein solutions starts locally to appear. This indicates that the above transformation may be a result of reduction of the hydration by electrolyte. Thus, the aggregation should be mediated by hydrophobic interaction, though hydrophilic interaction may also be responsible. It is shown in Fig. 1 in comparison with freezing temperature.

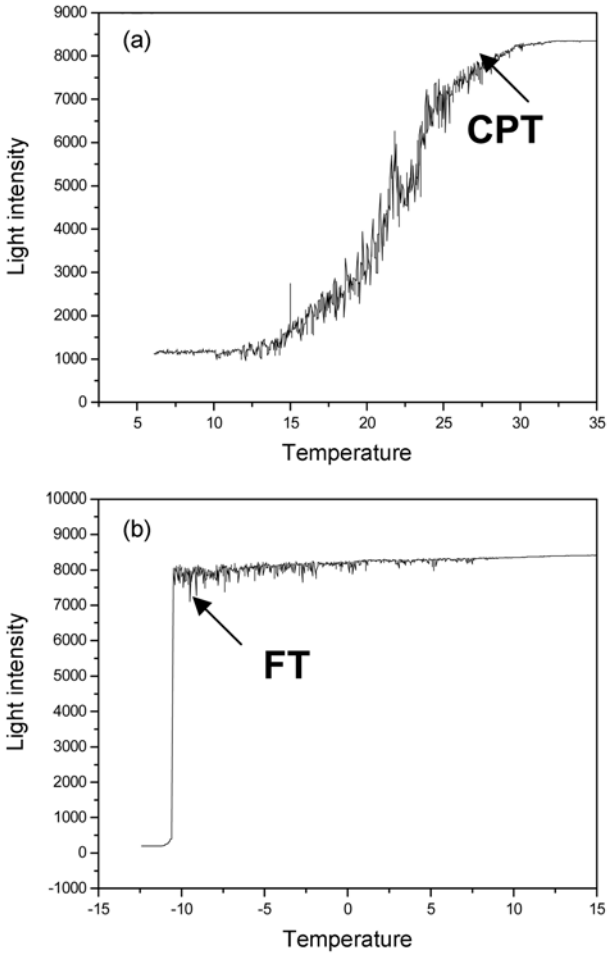

Fig. 1. Distinction between cloud-point temperature and freezing temperature. (a) BSA NaCl 0.2 M at pH 7.2; (b) Ovalbumin $NaNO_3$ 0.1 M at pH 7.2. A typical result for temperature determined by TOA technique is the difference that is the degree of decrease of light intensity. It is possible that the thermal diffusion is faster.

3. Model Development

The statistical thermodynamics on theories of fluids have been developed in terms of parameters characterizing the intermolecular forces for many types corresponding to different molecular models, such as the hard-sphere (HS) potential, the square-well (SW) potential, the Lennard-Jones (LJ) potential, the Sutherland potential, and the Kihara potential [28]. However, these potential functions are difficult to satisfy realistic requirements simultaneously [29, 30]. The SW potential is widely used for the intermolecular potential function with because of the simplicity of a mathematical model,

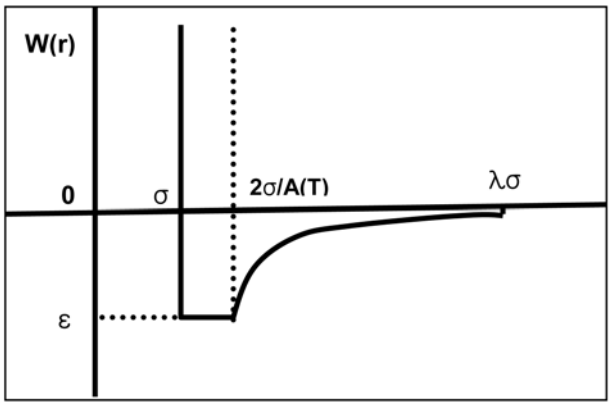

Fig. 2. A generalized Lennard-Jones potential model.

but it is known to be empirical in nature and not feasible due to a discontinuity. The LJ potential is able to represent intermolecular forces for various kinds of real-fluid. However, it implies that if two molecules have very high kinetic energy, they may be able to interpenetrate to separations smaller than the collision diameter, and the required integration is very complicated. In this study, we employ the LJ potential having a general shape to broaden its applicability to many different types of fluids. We reported a GLJ potential that can cover various interaction ranges [31], which is adjusted by a temperature-dependent parameter, but is still simple in mathematical form for spherically symmetrical and chemically identical molecules. It is expressed in Fig. 2 and as follows:

$$W(r)=\begin{cases}\infty & (0<r<\sigma)\\ -\varepsilon & (\sigma<r<2\sigma/A(\tilde{T}))\\ \dfrac{\varepsilon}{1-A(\tilde{T})\left(\dfrac{r}{\sigma}\right)} & (2\sigma/A(\tilde{T})<r<\lambda\sigma)\\ 0 & (r>\lambda\sigma)\end{cases} \tag{1}$$

where W(r) is the perturbation protein-protein potential, r is the center-to-center distance between two adjacent molecules, σ is the collision diameter, λ is reduced well width, ε is the minimum potential energy, $\tilde{T}=kT/\varepsilon$ is the reduced temperature with Boltzmann constant k, and $A(\tilde{T})$ is the temperature-dependent parameter that is determined from the computer simulation data for the compressibility factor. This equation is obviously more realistic and flexible than those of previously mentioned potential functions as the value of $A(\tilde{T})$ is adjusted with diverse conditions in addition to the parameters, σ and ε. See the appendix for further details.

The equation of state is defined in this section in terms of the Helmholtz energy per mole that represents hard-sphere interactions, i.e., GLJ potential. For obtaining the Helmholtz energy from a pressure-explicit EOS is

$$\frac{A}{NkT}=\frac{A^0}{NkT}+\frac{4\eta-3\eta^2}{(1-\eta)^2}+\frac{\rho_p U}{2kT} \tag{2}$$

where $A^0(T)$ is the Helmholtz energy at standard state. $\rho_p=N/V$ is the number density, N is the number of molecules, T is the absolute temperature, V is the volume of the system, $\eta=\pi\rho_p\sigma_p^3/6$ is the packing fraction, σ_p is protein diameter, U is the perturbation energy per unit density. The second term on the right hand side represents the Carnahan-Starling model for a hard sphere fluid, and the last term is modeled to the dispersion or perturbation part. By differentiating the Helmholtz energy with respect to the packing fraction in the system, the expressions for the chemical potential can be obtained.

$$\frac{\Delta\mu}{kT}=\frac{\partial}{\partial\eta}\left(\eta\frac{\Delta A}{NkT}\right)_{T,V,N_{i\neq k}}=Z^{hs}+Z^{disp}=Z \tag{3}$$

where $Z=P/(\rho_p kT)$ is the compressibility factor of the system, P is the pressure. To determine liquid-liquid phase coexistence, we employ the conventional conditions in the supernatant and dense phase, s and d, corresponding to coexisting at equilibrium.

$$\Delta\mu^s=\Delta\mu^d \tag{4}$$

$$P^s=P^d \tag{5}$$

At a given temperature, chemical potential μ and pressure P are functions of packing fraction (or number density) and the interaction energy. The dense phase, which is not known, is obtained from liquid-liquid phase coexistence. The perturbation energy can be obtained from the following relationship, which employs the GLJ potential by the function $A(\tilde{T})$.

$$U=4\pi\int W(r)r^2dr=-\frac{4\pi\varepsilon\sigma_p^3}{3}\left[\frac{\{3\ln(\lambda A-1)-4\}}{A^3}+\frac{3\lambda}{A^2}+\frac{3\lambda^2}{2A}-1\right] \tag{6}$$

4. Osmotic Pressure

Osmotic pressure, a phenomenon frequently encountered in nature, is a thermodynamic property used in the study of liquid solutions in physical chemistry. It was developed by using the van't Hoff equation analogous to the ideal-gas equation. Many researchers have reported osmotic pressures of different aqueous solution conditions containing proteins [32-39]. They also yielded an osmotic second virial coefficient which characterizes the anisotropic structure or orientation or intermolecular associations due to molecular interactions [40-42]. The interaction is usually based on the McMillan-Mayer virial equation [43] using the potential of mean force. Their objective is successful model representation of thermodynamic properties, such as osmotic pressure, virial coefficient, internal energy etc., of protein solutions. Our CPT was used to predict osmotic pressure by the calculated protein interaction energy from the MPHSC model. For an aqueous protein solution, Wu et al. [44] reported the osmotic compressibility EOS of the following expression. This model gives a semi-quantitative description of the osmotic pressure of protein solution at low salt concentration.

$$\frac{\pi}{\rho_p kT}=\frac{2}{\rho_p}\left\{\left[\left(\frac{z_p\rho_p}{2}\right)^2+\rho_s^2\right]^{1/2}-\rho_s\right\}+\frac{1+\eta+\eta^2-\eta^3}{(1-\eta)^3}+\frac{\rho_p U}{2kT} \tag{7}$$

where π is the osmotic pressure, z_p is the charge valence of protein and ρ_s is the number density of salt in the solvent. In this equation, the first term comes from the Donnan effect, which provides a simple correction due to the difference in salt solution, that is negligible at high salt concentration or at low protein charge, i.e., it takes into account the uneven distribution of small ions between the two chambers of the osmometer. Moreover, Wu et al. [44] reported that

the charge valence of protein depends on the ionic strength, which can only be found by potentiometer titration. Therefore, we assume that the charge valence of protein is independent of I in this work.

To calculate the osmotic pressure, the interaction energy parameters of a given solution with salt are determined from the experimental CPT data and expressed as quadratic function of ionic strength, and no additional adjustable model parameters are added.

RESULTS AND DISCUSSION

We have performed a symmetric investigation of liquid-liquid phase separation of aqueous protein solutions to explore the role of salt ions on protein interactions. There are several factors that should be considered to express the phase behavior of aqueous protein solutions. In this paper, thermodynamic models are developed for electrolyte effect of phase separation of aqueous protein solutions. We fixed the experimental conditions like pH and protein shape, etc. Tables 1 and 2 show the measured CPT of ovalbumin and BSA solutions at pH 7.2, respectively, and the protein concentration is fixed at 87 g/L. To demonstrate the effects of salt type and concentration on liquid-liquid phase separation and to determine phase separation boundary, the trends of measured CPTs are displayed in Figs.

Table 1. Experimental cloud-point temperatures for ovalbumin at pH 7.2 and 25 °C

Salt type	Salt concentration (M)	Cloud-point temperature (°C)
NaCl	0.1	10.8
	0.2	27.6
	0.3	34.7
	0.4	35.4
$NaNO_3$	0.15	11.0
	0.2	16.4
	0.3	28.4
	0.4	33.9
NH_4Cl	0.1	7.2
	0.15	18.8
	0.2	28.1
	0.3	30.0
	0.4	32.0
Na_2SO_4	0.1	10.7
	0.2	21.9
	0.3	25.5
	0.4	29.0
	0.5	28.8
	0.6	26.9
$(NH_4)_2SO_4$	0.1	19.5
	0.2	27.3
	0.3	32.1
	0.4	33.2
	0.5	33.3
$MgCl_2$	0.1	14.9
	0.2	23.1
	0.3	29.4
	0.4	30.5

Table 2. Experimental cloud-point temperatures for BSA at pH 7.2 and 25 °C

Salt type	Salt concentration (M)	Cloud-point temperature (°C)
NaCl	0.1	−0.4
	0.15	16.3
	0.2	28.6
	0.3	29.6
	0.4	31.1
$NaNO_3$	0.1	5.5
	0.2	13.4
	0.3	27.2
	0.4	35.6
NH_4Cl	0.1	10.3
	0.2	18.8
	0.3	32.1
	0.35	34.8
	0.4	36.8
Na_2SO_4	0.1	12.8
	0.2	21.3
	0.3	35.2
	0.4	38.0
$(NH_4)_2SO_4$	0.1	16.2
	0.2	23.4
	0.3	30.0
	0.4	30.5
	0.5	32.2
$MgCl_2$	0.1	7.3
	0.2	23.3
	0.3	33.4
	0.4	36.1

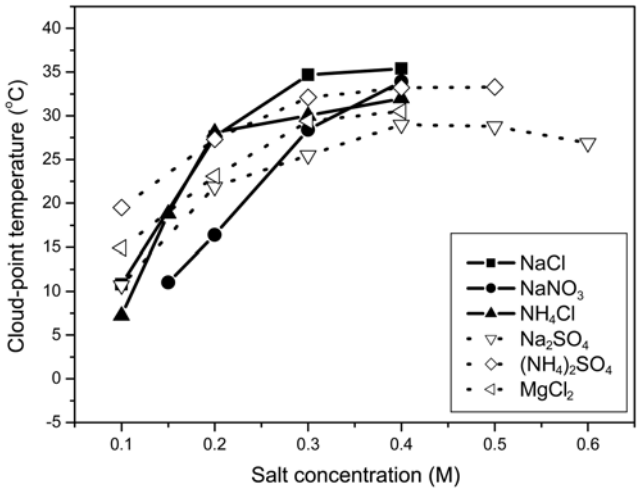

Fig. 3. Experimental cloud-point temperatures of ovalbumin solutions with various salts. The solid lines express monovalent ions; dotted lines express divalent ions.

3-6. CPTs were measured in 0.1-0.6 M ranges with various salt types. In Figs. 3 and 4, the effects of ionic strength are displayed. CPTs of lysozyme are reported by Park et al. [23] as shown in Fig. 7. Lyso-

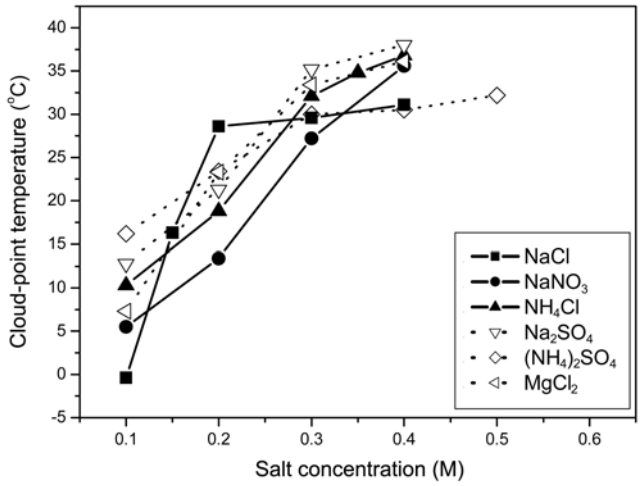

Fig. 4. Experimental cloud-point temperatures of BSA solutions with various salts. The solid lines express monovalent ions; dotted lines express divalent ions.

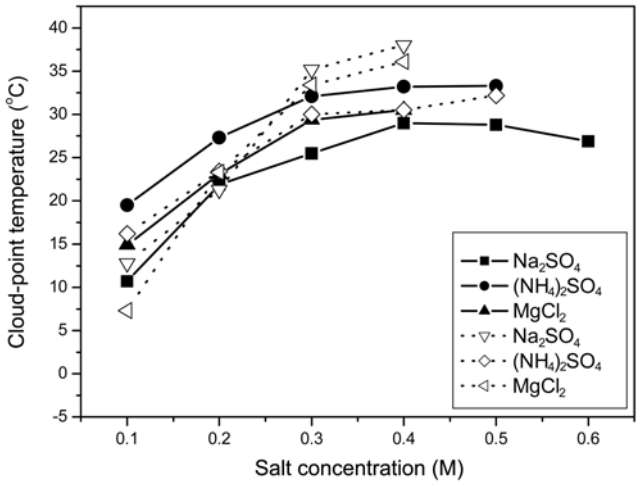

Fig. 6. Experimental cloud-point temperatures of ovalbumin and BSA solutions for three salts of different type with divalent ions. The solid lines express ovalbumin solutions; dotted lines express BSA solutions.

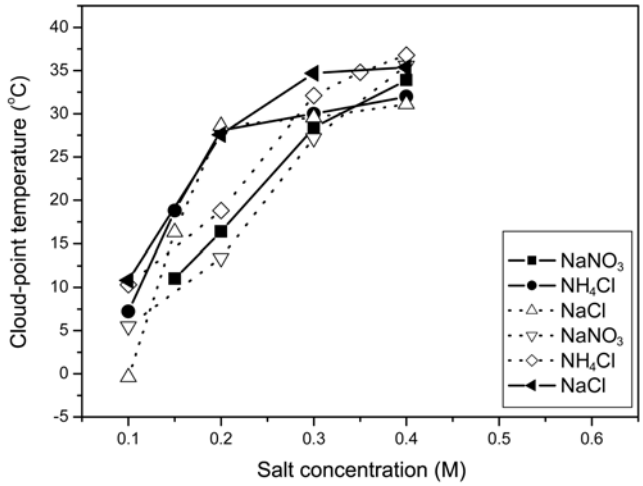

Fig. 5. Experimental cloud-point temperatures of ovalbumin and BSA solutions for three salts of different type of monovalent ions. The solid lines express ovalbumin solutions; dotted lines express BSA solutions.

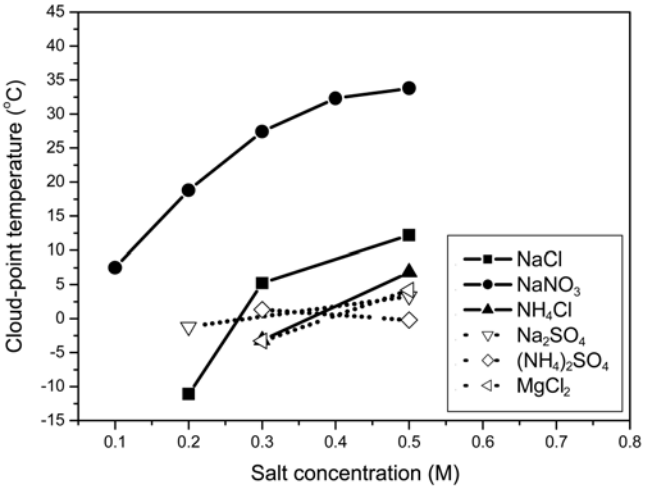

Fig. 7. Cloud-point temperatures of lysozyme solutions with various salts. The solid lines express monovalent ions; dotted lines express divalent ions. It is measured as 87 g/L protein solution at pH 7.0 by Park et al. [23].

zyme is well suitable for studies of protein phase behavior, since it is a robust and compact globular protein that is soluble in water over a broad concentration range.

Neal et al. [45] have shown that modeling proteins as smooth spheres may underestimate the excluded volume, and that the surface roughness may increase the excluded volume of the protein. Calculation of the excluded volume of the protein takes into account protein hydration by including an impenetrable layer of water thickness surrounding the protein. The thickness of the water layer significantly affects the protein interactions. The effective spherical diameter can be calculated from crystal structure dimensions; for the proteins considered here, lysozyme [46], ovalbumin [47] and BSA [48] have diameters of 34.4 Å, 50 Å and 62.5 Å, respectively. In this study, proteins are modeled as hard-spheres with uniform surface charge immersed in a continuous dielectric medium containing point charges depicting salt ions. The total net charge of protein due to the basic and acidic side residues of the protein can be estimated from hydrogen-ion titrations, which give the charge of the protein due to hydrogen-ion equilibria, when protein binds salt ions [48,49]. However the net charge is fixed at pH 7.2 for proteins considered here. We also classify types of solvation forces. Hydration forces occur when polar surface groups are desolvated. These forces are repulsive because the change in free energy for this process is positive, and work is required to remove water from polar groups. Hydrophobic forces are valid for describing attractions of results from desolvating non-polar groups such as surfaces of hydrophobic patches. These effects are granted only a right to the interactions going with protein types from CPTs.

Figs. 5 and 6 represent the effect of a variety of monovalent and divalent salts. For the monovalent ions, the CPT-curves increase rapidly with the salt concentration, and for divalent ions, as the salt con-

centration rises, the CPT-curves are displayed to a gentle ascent. Grisby et al. [50] reported the following that the effects of ionic strength on CPT depend strongly on the specific nature of anionic and cationic salts with solvation forces. Kosmotropic ions bind adjacent water molecules more strongly than those of water molecules itself. When kosmotropic ions are introduced into water, the entropy of the system decreases due to water structuring increased around ions. In contrast, when chaotropic ions are introduced into water, the entropy of the system increases because the water structuring around ions is less than that in salt-free water. This classification is related to the size and charge of ions. Taratuta et al. [51] reported that at high salt concentrations (>0.3 M), the specific nature of ions is much more important. However, we are not able to distinguish the specific nature of ions in low salt concentration ranges.

Protein interactions are known to be governed by many factors. In this study, we assume the energy parameter depends only on ionic strength I at the measured CPTs. Figs. 8 and 9 for sodium chloride represent the values of interaction energy plotted against ionic strength at pH 7.2. Grigsby et al. [50] reported ε/kT as a function of ionic strength that the trends are linear for monovalent salts, whereas the trends for divalent cationic salts show a quadratic dependence. For simplicity, we assume the solid lines to have parabolic shapes, and be quadratic functions of ionic strength. The energy parameters are listed on Tables 3 and 4 by correlating equations as a function of ionic strength for ovalbumin and BSA, respectively. In Fig. 9 for BSA, the correlating equation deviates from calculating energy value, but the deviation within error range is neglected. In Fig. 8 for ovalbumin, the correlating equation shows good agreement with experimental data. These figures may be extremely correlated expressions in low ionic strength range, but we were able to obtain the

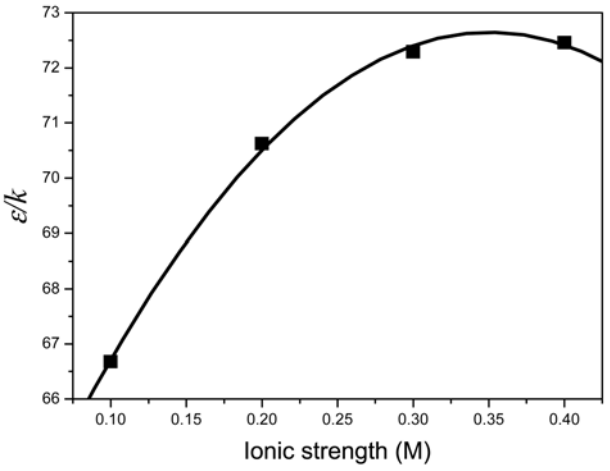

Fig. 8. Calculated values of energy parameter, ε/k, for 87 g/L ovalbumin solution plotted against ionic strength of sodium chloride at 25 °C and pH 7.2 (ε/k=61.03531+66.25403I−94.5145I^2).

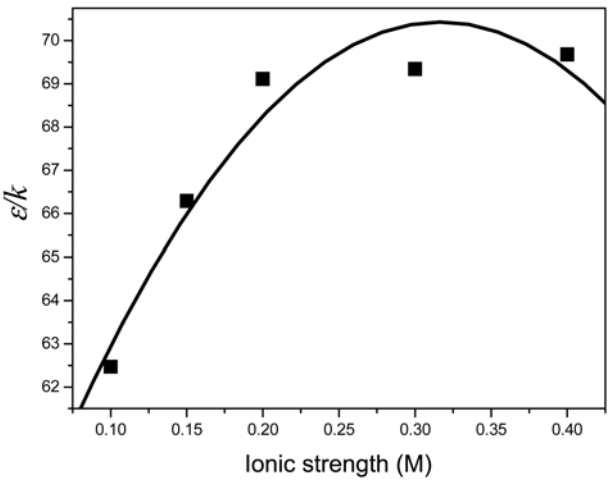

Fig. 9. Calculated values of energy parameter, ε/k, for 87 g/L BSA solution plotted against ionic strength of sodium chloride at 25 °C and pH 7.2 (ε/k=54.43424+100.96909I−159.37989I^2).

Table 3. Relation between the energy parameter ε/k and ionic strength I for ovalbumin

Salt type	ε/k=a+bI+cI^2
NaCl	ε/k=61.03531+66.25403I−94.5145I^2
$NaNO_3$	ε/k=60.34349+49.13208I−49.07609I^2
NH_4Cl	ε/k=59.8907+73.55948I−111.87756I^2
Na_2SO_4	ε/k=64.10093+30.74486I−33.8383I^2
$(NH_4)_2SO_4$	ε/k=66.36686+27.08818I−32.03636I^2
$MgCl_2$	ε/k=64.68664+33.30998I−41.682I^2

Table 4. Relation between the energy parameter ε/k and ionic strength I for BSA

Salt type	ε/k=a+bI+cI^2
NaCl	ε/k=54.43424+100.96909I−159.37989I^2
$NaNO_3$	ε/k=61.41858+22.41124I+2.86125I^2
NH_4Cl	ε/k=61.70218+32.71954I−22.438I^2
Na_2SO_4	ε/k=61.94504+36.81528I−32.62775I^2
$(NH_4)_2SO_4$	ε/k=63.97402+25.73368I−27.96043I^2
$MgCl_2$	ε/k=58.95861+60.16204I−76.12475I^2

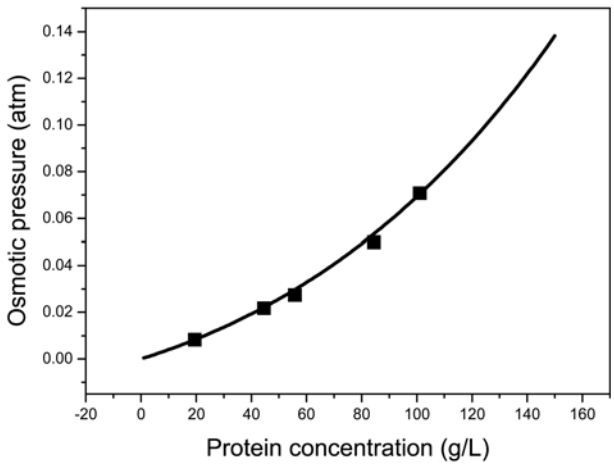

Fig. 10. Calculated and measured osmotic pressures of BSA solution at 1M salt concentration of sodium chloride. The solid curve is the calculated osmotic pressure based on theoretical considerations of molecular interactions. Data are reported by Wu et al. [44].

desired results within this range.

Very few publications have investigated the osmotic pressures of BSA and ovalbumin at high concentrations with sodium chloride, and these studies are based on most works reported previously by Vilker et al. [48]. We observed the osmotic pressures of aqueous protein solutions from correlating equations of the other salts as well as sodium chloride. In Fig. 10, BSA solution with sodium chloride is plotted against the protein concentration at pH 7.2. The dark squares are experimental data from Wu et al. [44]. Solid lines are calculated values from Eq. (7), and the required parameters to calculate the osmotic pressures are already determined from the computer simulation data for the compressibility factor or experimental CPT data of binary protein solutions in previous sections. It gives a good agreement with experimental data in low protein concentrations, despite relatively high salt concentrations. Osmotic pressure of BSA solution is predicted at 0.15 M of sodium chloride in Fig. 11. The deviation appears in the high protein concentration range but the trends follow the entire concentration range. Figs. 12 and 13 show the calculated osmotic pressures for ovalbumin/NaCl solution by using the same model. The dark squares are experimental data reported by Yousef et al. [34-36]. These figures show that the GLJ potential model deviates in the high concentration range, while it agrees fairly well with experimental data in the low range.

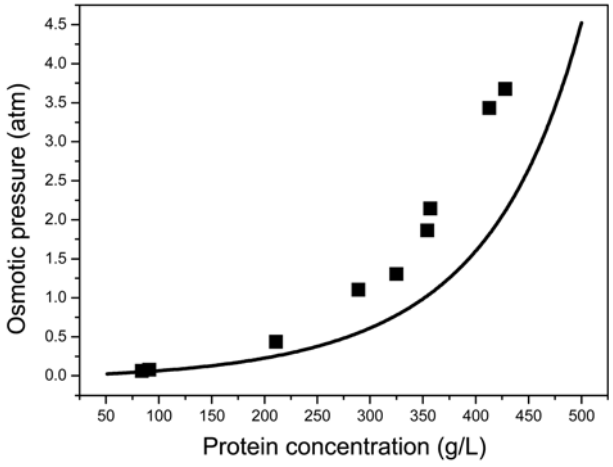

Fig. 11. Osmotic pressure versus BSA concentration at 0.15 M salt concentration of sodium chloride. Data are from [35].

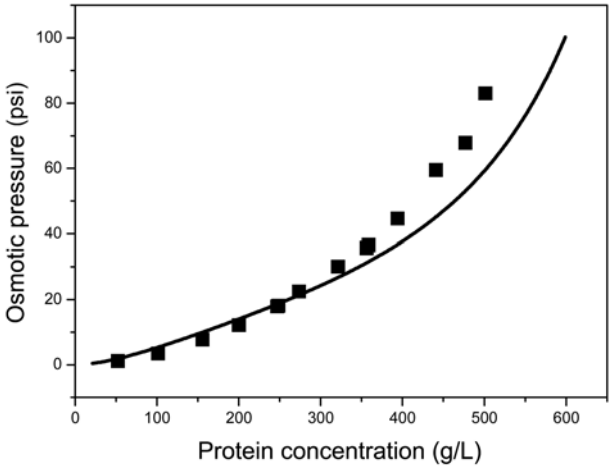

Fig. 12. Osmotic pressure versus ovalbumin concentration at 0.01 M salt concentration of sodium chloride. Data is taken from Yousef [36].

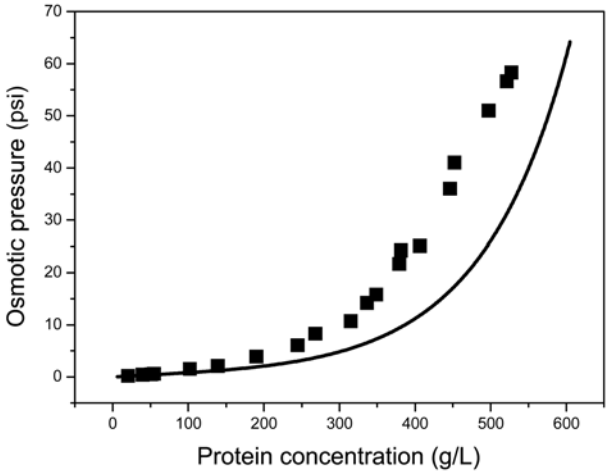

Fig. 13. Osmotic pressure versus ovalbumin concentration at 0.15 M salt concentration of sodium chloride. Data is taken from Yousef [36].

CONCLUSIONS

We used a TOA technique to measure CPT of ovalbumin/salt and BSA/salt solutions. The measured CPT provides detailed information on protein solutions for liquid-liquid phase boundary and phase behavior. In salt-induced protein solutions, the interaction between salt ions and protein molecules leads to the forces of protein aggregation or precipitation leading to liquid-liquid phase separation. We employed a potential function of generalized model to determine the interaction energy as a function of ionic composition. To provide a better understanding of the effect of electrolyte on protein solution, the specific and non-symmetric interaction forces that play a major role in determining liquid-liquid phase separation are needed to develop more accurate description of properties of concentrated solutions.

ACKNOWLEDGMENTS

This work was supported by Grant Number R01-2003-000-10261-0 from the Basic Research Program of the Korea Science and Engineering Foundation. In addition, the authors are grateful to Prof. J. M. Prausnitz from UC Berkeley.

REFERENCES

1. H. W. Blanch, J. M. Prausnitz, R. A. Curtis and D. Bratko, *Fluid Phase Equilib*., **194**, 31 (2002).
2. F. W. Tavares, D. Bratko, A. Striolo, H. W. Blanch and J. M. Prausnitz, *J. Chem. Phys*., **120**, 20 (2004).
3. C. Hass and J. Drenth, *J. Phys. Chem. B*, **102**, 4226 (1998).
4. R. K. Scopes, *Protein purification: Principles and practice*, Springer-Verlag, New York Inc. (1982).

5. N. Asherie, A. Lomakin and G. B. Benedek, *Phys. Rev. Lett*., **77**, 4832 (1996).
6. M. L. Broide, T. M. Tominc and M. D. Saxowsky, *Phys. Rev. E*, 6 (1995).
7. S. G. Kim, S. H. Kong, Y. C. Bae and S. J. Kim, *Macromole. Research*, **11**, 241 (2003).
8. P. Flory, *Principles of polymer chemistry*, Cornell University Press, Ithaca (1971).
9. W. M. Gelbart, A. Ben-Shaul and D. Roux, *Michelles, membranes, microemulsions, and monolayers*, Springer-Verlag, New York (1994).
10. P. R. tenWolde and D. Frenkel, *Science*, **277**, 1975 (1997).
11. L. A. M. Rupert, *J. Colloid Int. Sci*., **153**, 92 (1992).
12. F. Rothstein, *In protein precipitation process engineering*, R. G. Harrion, Ed., Dekker, New York (1994).
13. S. G. Kim and Y. C. Bae, *Macromole. Research*, **11**, 53 (2003).
14. D. E. Kuehner, H. W. Blanch and J. M. Prausnitz, *Fluid Phase Equilib*., **116**, 140 (1996).
15. F. Fornasiero, J. Ulrich and J. M. Prausnitz, *Chem. Eng. Pro*., **38**, 463 (1999).
16. J. Jiang and J. M. Prausnitz, *J. Phys. Chem. B*, **103**, 5560 (1999).
17. W. Liu, D. Bratko, J. M. Prausnitz and H. W. Blanch, *Biophys. Chem*., **107**, 289 (2004).
18. J. J. Grigsby, H. W. Blanch and J. M. Prausnitz, *J. Phys. B*, **104**, 3645 (2000).
19. M. Malfois, F. Bonnet, L. Belloni and A. Tardieu, *J. Chem. Phys*., **105**, 3290 (1996).
20. R. A. Curtis, J. Ulrich, A. Montaser, J. M. Prausnitz and H. W. Blanch, *Biotech. Bioeng*., **79**, 4 (2002).
21. R. A. Curtis, J. M. Prausnitz and H. W. Blanch, *Biotech. Bioeng*., **57**, 1 (1998).
22. U. W. Gedde, *Polymer physics*, Chapman and Hall (1995).
23. E. J. Park and Y. C. Bae, *Biophys. Chem*., **109**, 169 (2004).
24. G. N. Malcolm and J. S. Rowlinson, *Trans. Faraday Soc*., **53**, 921 (1967).
25. R. C. Mackenzie, *Thermochimica Acta*, **28**, 1 (1979).
26. R. C. Mackenzie, *Talanta*, **16**, 1227 (1969).
27. R. C. Mackenzie, C. J. Keattch, D. Dollimore, J. A. Forrester, A. A. Hodgson and J. P. Redfern, *Talanta*, **19**, 1079 (1972).
28. J. M. Prausnitz, R. N. Lichtenthaler and E. G. D. Azevedo, *Molecular thermodynamics of fluid-phase equilibria*, 3rd Ed., Prentice-Hall PTR (1999).
29. S. M. Walas, *Phase equilibria in chemical engineering*, Butterworths, Boston, MA (1985).
30. S. Shen and B. C.-Y. Lu, *Fluid Phase Equilib*., **84**, 9 (1993).
31. S. H. Choi and Y. C. Bae, *Physica. A*. (2005), submitted.
32. F. Cousin and V. Cabuil, *J. Mole. Liquid*, **83**, 203 (1999).
33. B. W. McCarty and E. T. Adams, *J. Biophys. Chem*., **28**, 149 (1987).
34. A. P. Minton, *Biophys. Chem*., **57**, 65 (1995).
35. M. A. Yousef, R. Datta and V. G. J. Rodgers, *J. Colloid Int. Sci*., **197**, 108 (1998).
36. M. A. Yousef, R. Datta and V. G. J. Rodgers, *J. Colloid Int. Sci*., **207**, 273 (1998).
37. M. A. Yousef, R. Datta and V. G. J. Rodgers, *J. Colloid Int. Sci*., **243**, 321 (2001).
38. D. A. Amos, J. H. Markels, S. Lynn and C. J. Radke, *J. Phys. Chem. B*, **102**, 2739 (1998).
39. R. J. Zimmerman, K. M. Kanal, J. Sanders, I. L. Cameron and G. D. Fullerton, *J. Biochem. Biophys. Methods*, **30**, 113 (1995).
40. B. L. Neal, D. Asthagiri, O. D. Velev, A. M. Lenhoff and E. W. Kaler, *J. Cryst. Growth*, **196**, 377 (1999).
41. Y. U. Moon, C. O. Anderson, H. W. Blanch and J. M. Prausnitz, *Fluid Phase Equilib*., **168**, 299 (2000).
42. R. A. Curtis, C. Steinbrecher, M. Heinemann, H. W. Blanch and J. M. Prausnitz, *Biophys. Chem*., **98**, 249 (2002).
43. W. G. McMillan Jr. and J. E. Mayer, *J. Chem. Phys*., **13**, 276 (1945).
44. J. Wu and J. M. Prausnitz, *Fluid Phase Equilib*., **155**, 139 (1999).
45. B. L. Neal and A. M. Lenhoff, *AIChE J*., **41**, 1010 (1995).
46. D. E. Kuehner, H. W. Blanch, C. Heyer, C. Ramsch, U. M. Fornefeld and J. M. Prausnitz, *Biophys. J*., **73**, 3211 (1997).
47. P. E. Stein, A. G. W. Leslie, J. T. Finch, W. G. Turnell, P. J. McLaughlin and R. W. Carrell, *Nature*, **347**, 99 (1990).
48. V. L. Vilker, C. K. Colton and K. A. Smith, *J. Colloid Int. Sci*., **79**, 548 (1981).
49. J. T. Edsall, *Proteins as acids and bases*, in: E. J. Cohn, J. T. Edsall, Eds., Proteins, Amino acids and Peptides, Reinhold Publishing Corp., New York (1943).
50. J. J. Grigsby, H. W. Blanch and J. M. Prausnitz, *Biophys. Chem*., **91**, 231 (2001).
51. V. G. Taratuta, A. Holschbach and G. M. Thurston, *J. Phys. Chem*., **94**, 2140 (1990).

APPENDIX(a). DETERMINATION OF A($\tilde{T}$)

We assume that A($\tilde{T}$) is dependent on temperature and obtained from the computer simulation data for the compressibility factor at various temperatures [30]. In the figure, calculated values of A($\tilde{T}$) are plotted against the reduced temperature. To simply correlate with simulation data, A($\tilde{T}$) is suggested:

$$A(\tilde{T}) = \frac{1.761 - 1.579\tilde{T}}{1 - \tilde{T}} \tag{A1}$$

When compared with calculated values of A($\tilde{T}$), Eq. (A1) reproduces those values fairly well.

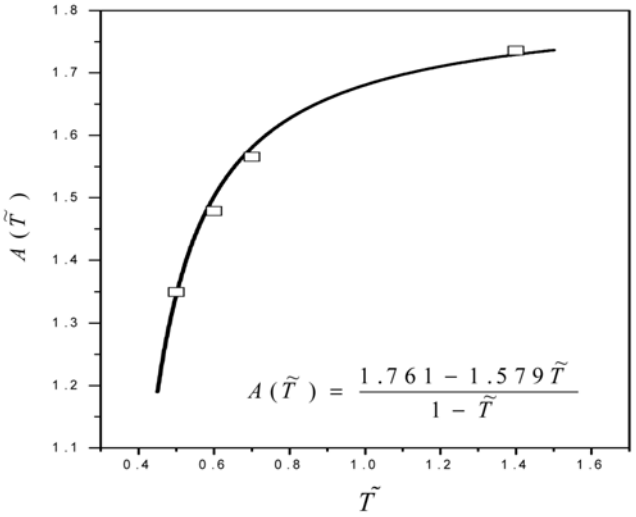

Fig. Calculated values of A($\tilde{T}$) plotted against A($\tilde{T}$).